Bollettino di Geofisica Teorica ed Applicata Vol. 58, n. 3, pp. 169-180; September 2017
DOI 10.4430/bgta0197

Controlled laboratory test for the investigation of LNAPL contamination using a 2.0 GHz ground penetrating radar

A.H. Mansi[1], M.P. Castillo[2] and G. Bernasconi[3]

[1] *Department of Civil and Environmental Engineering, Politecnico di Milano, Italy*
[2] *Environmental and Geomatics Engineering, Politecnico di Milano, Italy*
[3] *Department of Electronics, Information, and Bio-engineering, Politecnico di Milano, Italy*

(Received: January 30, 2017; accepted: July 5, 2017)

ABSTRACT Groundwater is an important source of fresh water and, consequently, its quality should be properly monitored. Different contaminants can be identified with different types of equipment and/or measurement procedures. Fuel oil contamination forms a "floating" layer over the water table, which has different electrical properties, therefore electromagnetic techniques can be used to image such contaminants. This paper presents a scale-laboratory test where a 2.0 GHz ground penetrating radar (GPR) is used to assess a controlled-fuel oil injection in a shallow sand tank setup. The test examined several scenarios involving different levels of water saturation and fuel oil contamination. The increase of water content produces a reduction of EM wave propagation velocity, moving some fixed/reference targets to higher reflection times. We use simplified relations to obtain approximated dielectric permittivity values, where the inverted results are consistent with those available in the literature for similar scenarios. Rather than suggesting a true quantitative procedure, these observations could be exploited in a qualitative long-term monitoring strategy in common field situations where a contaminant enters a soil matrix and moves through its pore spaces. Finally, the integration of GPR measurements with other monitoring techniques could increase the reliability of the interpretation and the sensitivity to the contaminant concentration.

Key words: ground penetrating radar, groundwater contamination, LNAPL, hydrocarbon contamination.

1. Introduction

The use of geophysical methods [ground-penetrating radar (GPR), electromagnetic induction (EM), and electrical resistivity] has been historically linked to the investigation of the subsurface (Hoover *et al*., 1992). Moreover, near-surface geophysics has aided several groundwater investigations, being used for mapping depth and thickness of aquifers and aquitards as well as for mapping and tracing contaminations. Porsani *et al*. (2004) conducted a GPR survey in order to evaluate the extension of a contaminant plume and from the obtained profiles, it was possible to understand its migration patterns. Likewise, Olofsson *et al*. (2005) attempted to identify the spreading pattern of a contaminant plume at a landfill by using a combination of geophysical measurements, including GPR and Very Low Frequency (VLF) with chemical analyses. The

combined approach yielded valuable results that allowed them to estimate the extension of the contaminated groundwater.

GPR is a state-of-the-art geophysical method that provides a high-resolution image of the near subsurface and it has been applied in several studies regarding the detection of hydrocarbon contaminants in spill sites and in controlled environments. Controlled environments can be used to test the effectiveness of GPR to map liquid contaminants, as in the surveys carried out by Daniels *et al*. (1995), Bano *et al*. (2009) and Capozzoli *et al*. (2012). In their controlled surveys, Daniels *et al*. (1995) found a clear GPR anomaly in the containers where the porous material was saturated with diesel fuel. Bano *et al*. (2009) carried out a test using a sandbox to recreate an aquifer. The use of the GPR proved that there is a clear and obvious effect of the light non-aqueous phase liquid (LNAPL) injection translated into travel time. Finally, Capozzoli *et al*. (2012) also conducted a test in a controlled environment concluding that GPR measurements can detect changes in permittivity values after the contaminant injection. One of the best features of the GPR is the resolution of the mapping, which excels that of the lower frequency EM methods, but only for limited penetration depths, depending on the frequency of the antenna (Ludwig *et al*., 2009). Additionally, the data acquisition is a fast process that allows the surveyor to carry out more measurements in a quick manner with an adequate temporal resolution in case of rapid changes in the subsurface configuration: for instance, water content monitoring and other similar applications (Takahashi *et al*., 2012).

The relevance of this method for the detection of hydrocarbon compounds lies in the possibility of measuring the reflection of the water table, especially when there is a sharp change in the moisture content between the vadose and the saturated zones. When a contaminant enters the soil, it interacts with the water present in it, producing a change in the electrical properties.

The use of GPR for hydrocarbon and LNAPL detection is common and particularly popular, although it is not a straightforward method (Marcak and Gołębiowski, 2008) and its success is limited, which motivates the investigation of advances with inductive and galvanic systems (Pellerin, 2002).

In general, GPR is not able to identify a particular contaminant but how the groundwater changes with it (Brewster and Annan, 1994). The physical property of interest in a GPR acquisition is the relative dielectric permittivity, a measure of the 'polarisability'[1] of a material. According to (Peplinski *et al*., 1995), both the real and imaginary components of the dielectric permittivity can be empirically computed for soils, because both are functions of the volumetric moisture content of the soil, the bulk density and the specific density of the solid soil particles. Other empirical constants are involved, too, and they depend mostly on the soil type and composition. Dielectric permittivity varies notably in the materials of interest (air: ε_r=1, air-dry sand: ε_r=2-6, water: ε_r=80, and LNAPL: ε_r=1.8-3) (Daniels *et al*., 1995; Cassidy, 2007). Sometimes the attenuation of the GPR signal is exploited to interpret the properties of the subsurface as well as the nature of the fluids present in the soil pores.

Atekwana *et al*. (2000) studied a plume of LNAPL contaminant produced by fifty years of leakage into a site. The contaminants became conductive as a result of the degradation processes. On the other hand, Orlando (2002) presented the results of a test conducted in an area with a variable thickness of LNAPL. The study area was contaminated with both gasoline and diesel fuel

[1] Polarisability refers to the ability of a material to form instantaneous dipoles.

due to a damaged hydrocarbon pipeline. The results showed how it is not possible to establish rules about the behavior of the signal in regard to the LNAPL presence unless the analysis is based on the hydro-geological context of the contamination. This conclusion had also been reached by Atekwana *et al*. (2000) in the previous case, where the age of the contaminant plume determined a different behavior of the GPR response from other LNAPL mapping cases using GPR. Even though in theory hydrocarbons travelling in the subsurface change the electrical properties of their host medium, this change can take any shape and it is definitely a complex process. Contaminant plumes are expected to be highly variable with time (Benson *et al*., 1997) because many phenomena need to be taken into account. Biodegradation, for instance, has a lowering effect on resistivity values due to the increment in total dissolved solids (TDS). These are factors that might be taken into consideration depending on the age of the contamination.

The laboratory experiment proposed in this paper evaluates the performance of a 2.0 GHz frequency GPR system in the characterization of a shallow sand tank setup. The test encompasses different situations involving acquisitions for two different levels of water saturation and two acquisitions after the addition of fuel oil to one of the sides of the tank for comparison purposes.

We have processed the radar images to compare travel time and amplitudes of the reflections from the water table. The result is an increment of the two-way travel time for increasing water content and a high amplitude anomaly in the contaminated zone of the tank for the contaminated scenario, with an increasing amplitude roughly proportional to the volume of free-phase fuel oil injected. The high frequency of the antenna provided an outstanding resolution for the radargrams, and the wave velocity and relative dielectric permittivity of the materials have been estimated from their reflection profiles.

2. Description of the test

The test reconstructs a scaled model of the subsurface using a 78×56×42 cm rectangular transparent plastic container, filled with an unconfined, poorly graded, coarse-grained sand up to a level of about 30 cm. We made a granulometry/grain size distribution test on river sand. The results revealed that about 60% of the sample has a grain size between 0.5 and 4.0 mm (gravel, <9%; very coarse sand, ≅23%; and coarse sand, ≅38.4%), the rest is a mix of medium, fine and very fine sand. The porosity was estimated to be around 24%, which is in accordance with the literature for an unconsolidated sand.

The plastic container was divided into two identical compartments separated by a plastic wall perforated at the bottom to allow the flow of water and, consequently, to have a uniform water table in both compartments (Figs. 1a and 1c). The idea behind this separation is the evaluation of the difference in the GPR response when only one of the compartments is injected with fuel oil. Three PVC pipes were placed in the corners of the chambers as follows: two pipes for water injection with a total length of 44 cm and an internal diameter of 1.6 cm in both chambers, and a single pipe for oil leakage with a length of 20 cm. The water pipes were placed 1 cm above the bottom of the tank in both chambers, while the oil pipe was placed 12 cm above the bottom of the tank. The tank was mounted on a wooden frame before the tests. The contaminant employed was fuel oil No. 2, with a measured density of 0.8740 g/ml and a dielectric permittivity value of ε_r=2.7 (in accordance with the literature).

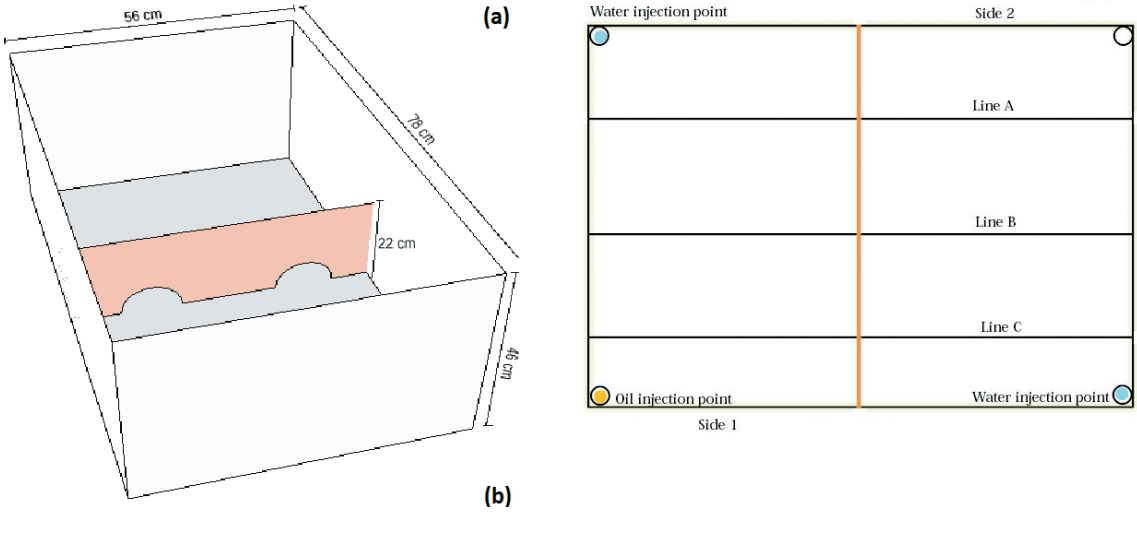

Fig. 1 - Features of the test: a) schematic representation of the geometry of the tank model used for the laboratory test; b) schematic representation of the configuration of the tank and survey line A, line B, and line C, as well as the oil and water injection points (top view); c) the realization of the schematic representation.

The GPR acquisitions were performed on three parallel lines (Figs. 1b and 1c), with a 2.0 GHz antenna. Each acquisition line has 52 equally separated traces of 20 ns each.

The first test involved the evaluation of the GPR signal during the addition of approximately 5.1 liters of water, which was divided into two approximately equal parts and simultaneously poured in the tank through both water pipes at a constant rate of about 0.01 litres/second (l/s). Such water volume accumulated a water table of approximately 8 cm above the bottom of the tank. The second test was carried out three days later, by adding 7.7 more litres of water, reaching a considerable water table of about 12.5 cm above the bottom of the tank. The third test was also carried out on the same day, after the previous test. The tank was displaced to an aired location causing the liquefaction of the soil. Some soil was removed from the tank leaving a saturated sample over which an oil lens was directly poured to produce a GPR acquisition in a supposed case of a "pancake model" in the subsurface. This also avoids the slow transport of the oil downwards and its subsequent lateral spreading, as if it had been poured over the surface of the vadose zone. Then, a new air-dry soil sample was added. During the GPR measurements, more fuel oil was

added at the same constant rate of 0.01 l/s through the oil pipe. Additional information about the experiment setup, the description of all the intermediate steps, and their corresponding results can be found in Castillo (2013). Fig. 1c shows a photo of the tank before an acquisition: the radar is moved manually along the lines on a plastic foil laying on top of the sand. This way of manual operation, the mobilization of the tank, the different measuring moments with respect to the transient or the steady state conditions of the water table, make the test not fully reproducible and can explain some variations in the images of reference targets (e.g., the metal rod). Moreover, test scalability refers to the geometrical inverse proportionality between GPR central frequency and the dimension of the test, although there could be additional effects due to the different response of the investigated media with respect to the frequency of the incident EM waves. However, the results are similar to the ones obtained by full-scale experimental procedures, and so this experiment can be considered a useful laboratory test for prototyping operation procedures.

The data acquisition was done using a constant offset configuration with an ALADDIN GPR (IDS) system full polar with an antenna frequency of 2.0 GHz, which allows a simultaneous acquisition of longitudinal polar or horizontal transmit and horizontal receive (HH) on channel 1 and transversal polar or vertical transmit and vertical receive (VV) on channel 2. The following parameters were taken into account: antenna frequency, antenna spacing and orientation, and recording time window, as it is specified for a common offset survey (Annan, 2005). Wave pulses are emitted at equidistant intervals and the main characteristic of this mode of acquisition is the efficient and fast way to obtain the data of the subsurface structures (Hubbard *et al.*, 2002; Ludwig *et al.*, 2009).

The data obtained were processed using the REFLEXW (Sandmeier) software to remove the noise, enhance the quality of the radargrams, and suppress unwanted diffraction from the frame of the tank. The implemented processing flow was the following:

- 1D bandpass frequency filter: a filter defined by four frequency values of a trapezoidal filter shape. The four values used were 800, 1000, 2800, and 3000 MHz;
- 2D background removal: a filter that removes an average trace within a chosen time or distance range. All the acquired data, 52 traces for each acquisition line, presented background reflections within the first few nanoseconds. The parameters of the filter required to specify a start and end time/distance for the computation of the average trace that will be subtracted. The data were acquired for an approximate interval of 20 ns and the background was removed for the first nanosecond (varying between 1.0 and 1.3 ns, depending on the data set) along the whole time/distance axis;
- static correction: a filter that moves the start time of each trace to match the start time of the trace with the position of the surface. The first significant arrival was determined and the resulting shift was less than 0.5 ns. Time drift was related to a small variation of the synchronization between transmitting and receiving antennas, probably caused by some thermal variation;
- diffraction stack migration: a process performed as a simple time back-propagation of the 2D profile in a constant velocity medium. The parameters are the summation width, or the number of traces over which there will be a summation, the velocity, calculated using the velocity adaptation tool to adapt pre-calculated hyperbolas to existing diffraction hyperbolas, and start time and end time (the time range over which the process will be applied);

- complex trace analysis: a processing step that makes use of the Hilbert transform to determine instantaneous attributes of a signal (instantaneous amplitude or envelope, instantaneous phase, and instantaneous frequency). The instantaneous amplitude was calculated for the profiles along line B for the two different oil thicknesses. We use this attribute as a reflection amplitude when comparing the different scenarios.

It must be pointed out that because of the high visibility of the reflections of the targets of interest without applying any "amplitude correction" and in order to perform the same processing for all the experiments, we decided not to apply any amplitude-related processing.

3. Analysis of the test

3.1. GPR response before water injection

Fig. 2 shows the processed radargrams of the tank before the water injection. The reflection of the bottom of the tank is at 4 ns (two-way arrival time).

A metal rod 10 cm long, 1 cm wide, and 0.2 cm thick was placed on top of the sand, perpendicular to line B and closer to line A than line C, in order to determine the two-way arrival time of the surface of the sand and to be used as a reference level for both time and depth (see the white arrow in Fig. 2b). For this reason, its diffraction is visible in the radargrams for lines A and B only.

Visual inspection reveals that the reflection of the bottom of the tank which is at a depth equal to 30 cm, corresponds to a two-way travel time of 4 ns, approximately. Then, the computed velocity is around 0.15 m/ns. Hence, it is possible to determine the dielectric permittivity of the air-dry sand before the water injection using the simplified formula (see Eq. 1) that relates the velocity of the wave to the dielectric permittivity of the media, which holds for good dielectric materials:

$$v_m = \frac{c}{\sqrt{\varepsilon_r}} \tag{1}$$

The value obtained, ε_r=4, is consistent with the literature (Davis and Annan, 1989).

3.2. GPR response after water injection

A time-lapse acquisition was done during the water inflow by placing the GPR near one of the water pipes. The water was poured at almost constant intervals for about 30 minutes: after each injection a radar acquisition was done, as the water content increases in the tank it reveals that the arrival time of the reflections from the bottom of the tank becomes greater, due to the corresponding overall decrease of the EM velocity (Fig. 3). The vertical discontinuities in Fig. 3 coincide with the starting of the recording.

The final profiles for the first test are displayed in Fig. 4. All the lines were acquired immediately after all the water (5.1 litres) had been added to the tank. At this point, the water table was in a transient state with a higher water column near the water pipes than in the centre of the tank. This resulted in a slower propagation of the GPR signal near the edges of the tank as seen in the reflection of the bottom of the tank in Fig. 4. However, after reaching the steady state condition, the water table was at about 22 cm below the surface (i.e., 8 cm above the bottom of the tank).

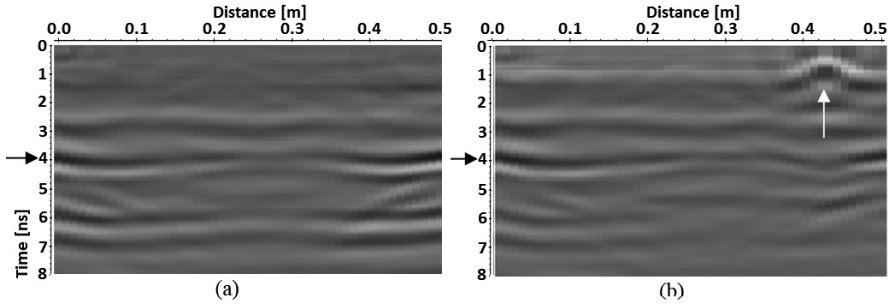

Fig. 2 - Profile along line B: a) before water injection; b) with a strong reflector that corresponds to a metal rod at the surface. The black horizontal arrows represent the bottom of the box and the white vertical arrow points at the diffraction from the metal rod. The tank was mounted on a wooden pallet with support wooden bars placed beneath the edges. The corresponding effect is a slight lateral amplitude variation at 6 ns.

The reflections of the radargrams were used to estimate the ground wave velocity: 0.065 m/ns, which has been used in Eq. 1 to compute a relative dielectric permittivity: 21.3 for water-saturated sand. Additionally, the volumetric water content of fully-saturated sand, equivalent to 24%, was used to estimate a dielectric permittivity of 12.7 using the Topp's equation (Topp *et al.*, 1980), which corresponds to a ground wave velocity of 0.084 m/ns. The results of both techniques are consistent with the values available in the literature (Mukhlisin and Saputra, 2013).

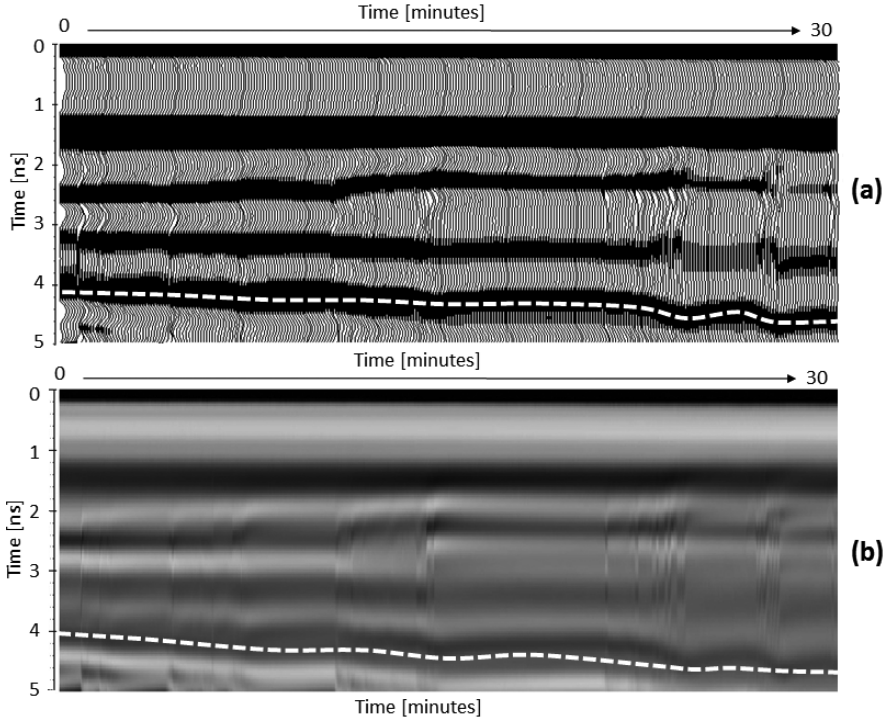

Fig. 3 - Time acquisition near one of the water pipes represented as: a) wiggle traces on the top panel; and b) gray-scale colorbar on the bottom panel. Both axes represent time. Y-axis represents arrival time (ns) while X-axis represents the increasing water content in the tank for increasing times, where the dry condition is displayed at time zero. The dotted white line represents the reflection of the bottom of the tank.

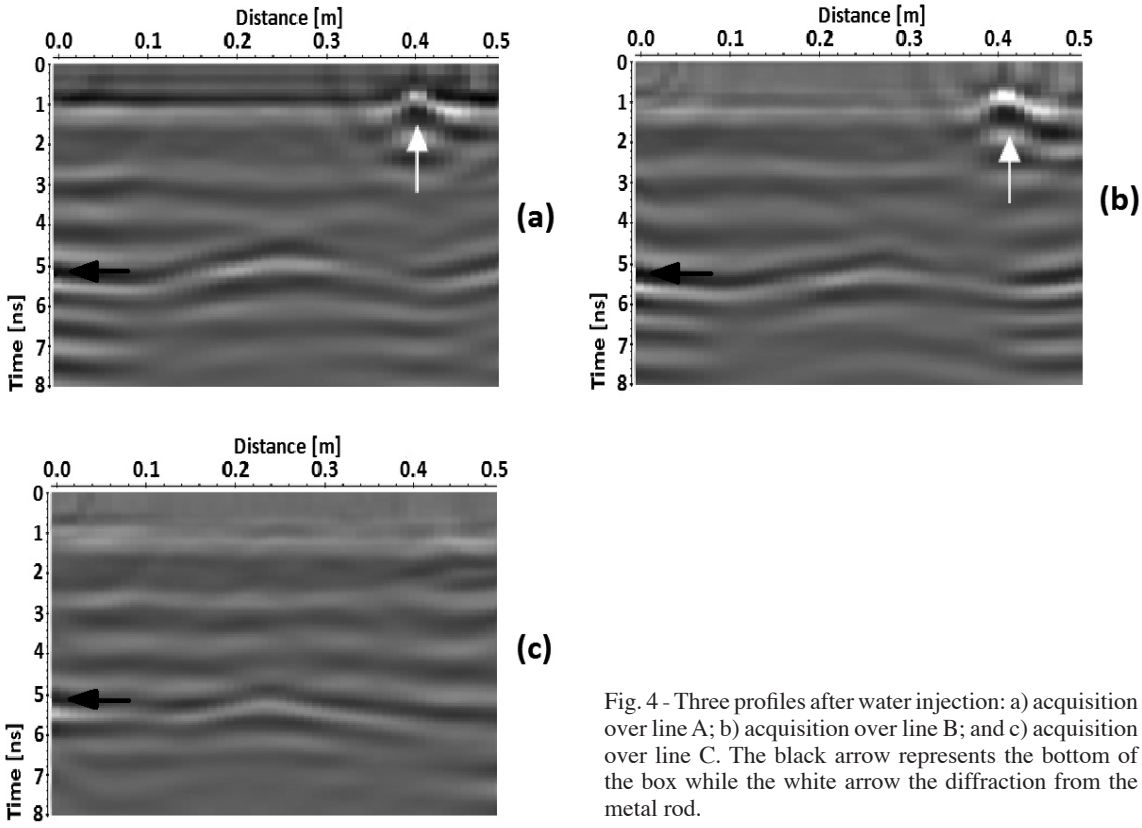

Fig. 4 - Three profiles after water injection: a) acquisition over line A; b) acquisition over line B; and c) acquisition over line C. The black arrow represents the bottom of the box while the white arrow the diffraction from the metal rod.

After the first test, the tank was allowed to settle for a few days in order to reach a steady state condition as seen in Fig. 5a. Then, in the second test, more water was added at the same constant rate of 0.01 l/s, and the radargram reported in Fig. 5b corresponds to the acquisition after the injection of a total volume of 13 litres of water. This corresponds to a water table at about 12.5 cm above the bottom of the tank.

The test proves that it is possible to link the moisture content with the arrival time of the reflections from the tank. In Fig. 5, the reflection of the bottom of the tank is visibly delayed in

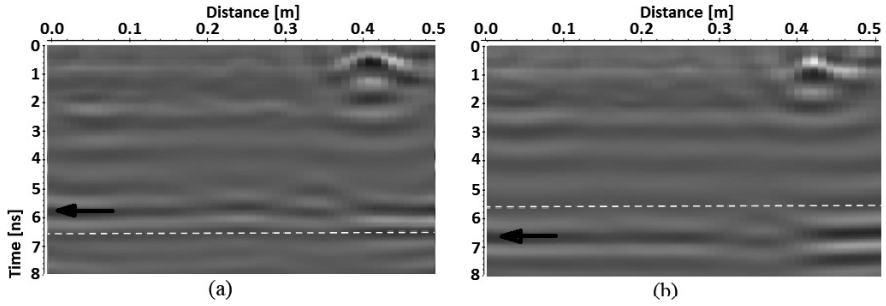

Fig. 5 - Profiles of the second test over line B: a) acquisition over line B after reaching the steady state water table after the first test; b) acquisition over line B after reaching the steady state water table after the full amount of water was added to the tank. The black arrow represents the bottom of the box while the dotted white line represents the location of the bottom on the other profile.

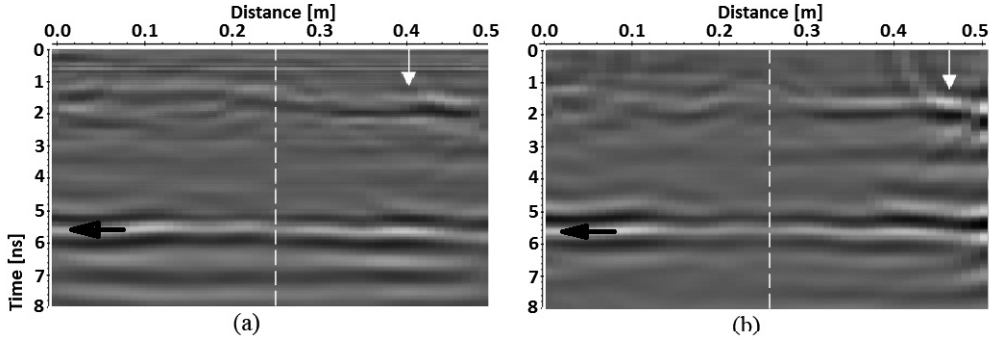

Fig. 6 - Profiles over line B: a) the first profile with a directly poured oil lens of 11 mm; b) the last profile after the total volume of oil had been injected (about 21 mm). The black arrow represents the bottom of the box and the white vertical arrow indicates the reflection produced by the fuel oil. The dashed white line represents the separation of the tank, between the uncontaminated (left) and contaminated (right) zones. The reflection of the oil-water interface is very noticeable in the contaminated zones on both cases.

association with the increase in water content in the soil sample. It is important to mention that such estimation can be done only when repeated GPR acquisitions (i.e., time lapse data) are available, and when it is possible to identify reference "fixed" targets.

3.3. GPR response after oil injection

The third test was conducted to evaluate the GPR response after approximately 0.6 liters of oil (i.e., a contaminated sand layer of 1.14 cm thickness) were directly poured over the water table only in the first compartment of the tank, while the other side was left undisturbed. After that, more air-dry sand was added to both sides. The depth of the water-saturated sand was about 12.5 cm (as it was before).

In a second instance, an additional volume of 0.5 litre of fuel oil was injected to the already contaminated compartment of the tank reaching a final contaminated layer of about 2.1 cm thickness.

We analyzed the first and last profiles along line B. The oil lenses in the two situations are slightly different: in the first profile, the oil lens is of about 11 mm after 0.6 litres of oil were poured over the first compartment. The second profile corresponds to the last radargram acquired for a final oil thickness of about 21 mm (corresponding to the additional volume of 0.5 litres). The comparison reveals a higher amplitude anomaly in the second profile (Fig. 6).

The most remarkable contrast found within each one of these profiles is the strong reflector located only in one of the sides of the tank, corresponding to the contaminated area. Starting next to the oil injection pipe and spreading laterally, there is a strong reflector that can be seen in all the radargrams recorded after the contaminant injection.

These radargrams were processed according to the processing flow described in section 2, including the use of the Hilbert transform to determine the instantaneous amplitude of the traces. The instantaneous amplitude is an attribute that represents the impedance contrast, which depends on the contrasts in electrical conductivity and dielectric permittivity of the medium (Hagrey, 2004).

Fig. 7 shows some profiles after the Complex Trace Analysis has been applied. The instantaneous amplitude is always positive and the appearance of the strong reflectors is a more noticeable

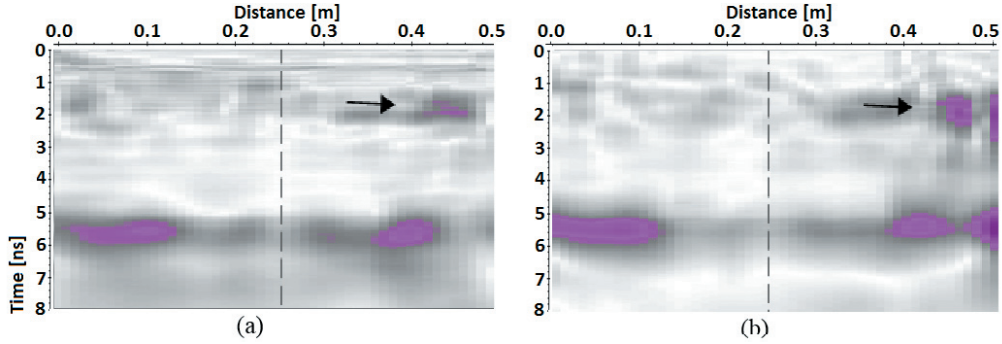

Fig. 7 - Instantaneous amplitude radargrams: a) for an oil thickness of 11 mm; b) for an oil thickness of 21 mm. The dashed line represents the separation of the tank, between the uncontaminated (left) and contaminated (right) zones. The arrow points to the amplitude anomaly from the oil lens. The reflections seen approximately at 6 ns coincide with the base of the tank given the corresponding distance estimated from their arrival time.

depiction of the anomalous amplitude. The instantaneous amplitude contrast is significant both between the uncontaminated zone and contaminated zone and between the different oil lens thicknesses.

The instantaneous amplitude values for the contaminated and uncontaminated zones were retrieved from the data for analogous points on both sides of the tank. This was done merely to gain an idea of the magnitude of the change that can be observed. The obtained values are listed in Table 1.

The comparison for the contaminated and uncontaminated zones reveals a significant change in instantaneous amplitude, which can reach values more than four times higher in the contaminated zone. The discrepancies in instantaneous amplitude of the uncontaminated compartment could be linked to the non-identical experimental conditions of the two measurement periods.

Table 1 - Comparison of the instantaneous amplitudes for the contaminated and uncontaminated zones.

Contaminated Zone			
Oil Thickness [mm]	Horizontal Distance [m]	Time [ns]	Instantaneous Amplitude
11	0.46	1.85	419
21	0.46	1.85	701
Uncontaminated Zone			
Oil Thickness [mm]	Horizontal Distance [m]	Time [ns]	Instantaneous Amplitude
	0.04	1.85	251
	0.04	1.85	168

4. Discussion

The results obtained in the aforementioned three tests are consistent with the outcome of similar test settings available in the literature (Daniels *et al.*, 1995; Capozzoli *et al.*, 2012). On the one hand, there is the effect of water content in the soil: due to its peculiar electromagnetic properties, water slows down the electromagnetic waves coming from the transmitter and the arrival time is significantly delayed for increasing water content. On the other hand, reflection amplitude

from the water table can be used as an indicator of a contamination: the injection of the first volume of the LNAPL (i.e., oil thickness of 11 mm), almost doubled the instantaneous amplitude values. Other authors have also achieved similar results that describe stronger amplitudes for the contaminated scenarios, with amplitudes approximately three times greater when LNAPL is present (Kim *et al*., 2000).

Finally, for a 2.0 GHz antenna in a medium with a velocity of 0.15 m/ns, the theoretical vertical resolution is around 2.0 cm. For our case, a sand with 24% porosity, a liter of fuel oil would correspond to more than 2 cm of contaminated sand above the water-saturated layer, which is of the same order of the radar resolution: as a result, after the second fuel injection test, the anomaly became evident and easily detectable.

5. Conclusions

We have presented a scale-experiment of GPR investigation in an LNAPL contaminated scenario, in order to gain an improved understanding of the behaviour of the GPR signal in response to a contaminant of a specific nature. Under these controlled circumstances, the contamination degree and the fluid migration within the tank are known, and therefore its electromagnetic response can be correctly assigned to the phenomena that are effectively taking place.

While the controlled environment setup allowed the detection of the contaminant (i.e., fuel oil) in the tank, the situation presented in this experiment can be far from a real case scenario. Rather than proposing a full scale quantitative procedure, the experiment shows a scaled-scenario that evidences the relevance of GPR for the prospecting of the near subsurface. Therefore, it supports the use of a continuous radar monitoring to track reflection amplitudes and EM propagation velocities and to link this information to the presence of certain contaminants and water saturation.

Integration of GPR measurements with other monitoring techniques is fundamental for the experimental calibration of the amplitude thresholds.

REFERENCES

Annan A.P.; 2005: *GPR methods for hydrogeological studies*. In: Rubin Y. and Hubbard S.S. (eds), Hydrogeophysics, Water Science and Technology Library, Springer, Dordrecht, The Netherlands, vol. 50, pp. 185-213, doi:10.1007/1-4020-3102-5_7.

Atekwana E.A., Sauck W.A. and Werkema D.D.; 2000: *Investigations of geoelectrical signatures at a hydrocarbon contaminated site*. J. Appl. Geophys., **44**, 167-180, doi:10.1016/S0926-9851(98)00033-0.

Bano M., Loeffler O. and Girard J.-F.; 2009: *Ground penetrating radar imaging and time-domain modelling of the infiltration of diesel fuel in a sandbox experiment*. Comptes Rendus Geosci., **341**, 846-858, doi:10.1016/j.crte.2009.08.002.

Benson A.K., Payne K.L. and Stubben M.A.; 1997: *Mapping groundwater contamination using dc resistivity and VLF geophysical methods - a case study*. Geophys., **62**, 80-86, doi:10.1190/1.1444148.

Brewster M.L. and Annan A.P.; 1994: *Ground-penetrating radar monitoring of a controlled DNAPL release: 200 MHz radar.* Geophys., **59**, 1211-1221, doi:10.1190/1.1443679.

Capozzoli L., Giampaolo V., Rizzo E., Votta M., Cucci P., De Biase M. and Straface S.; 2012: *Ground penetrating radar as a powerful tool for the study and the monitoring of LNAPL - contamination in the subsoil*. In: Proc. 31st Convegno Gruppo Nazionale Geofisica Terra Solida, Potenza, Italy, pp. 60-67, doi:goo.gl/WxcpXT.

Cassidy N.J.; 2007: *Evaluating LNAPL contamination using GPR signal attenuation analysis and dielectric property measurements: practical implications for hydrological studies*. J. Contam. Hydrol., **94**, 49-75, doi:10.1016/j.jconhyd.2007.05.002.

Castillo M.P.; 2013: *Using ground-penetrating radar in the investigation of LNAPL contamination within a controlled environment*. Master of Science, Thesis in Environmental and Geomatic Engineering, Politecnico di Milano, Milano, Italy, doi:10.13140/RG.2.1.3228.6565.

Daniels J., Roberts R. and Vendl M.; 1995: *Ground penetrating radar for the detection of liquid contaminants*. J. Appl. Geophys., **33**, 195-207, doi:10.1016/0926-9851(95)90041-1.

Davis J.L. and Annan A.P.; 1989: *Ground-penetrating radar for high-resolution mapping of soil and rock stratigraphy*. Geophys. Prospect., **37**, 531-551, doi:10.1111/j.1365-2478.1989.tb02221.x.

Hagrey S.A.; 2004: *GPR application for mapping toluene infiltration in a heterogeneous sand model*. J. Environ. Eng. Geophys., **9**, 79-85, doi:10.4133/JEEG9.2.79.

Hoover D.B., Heran W.D. and Hill P.L.; 1992: *The geophysical expression of selected mineral deposit models*. U.S. Geological Survey, Golden, CO, USA, Open file report 92-557, 129 pp.

Hubbard S., Grote K. and Rubin Y.; 2002: *Mapping the volumetric soil water content of a California vineyard using high-frequency GPR ground wave data*. The Leading Edge, **21**, 552-559, doi: https://doi.org/10.1190/1.1490641.

Kim C., Daniels J.J., Guy E.D., Radzevicius S.J. and Holt J.; 2000: *Residual hydrocarbons in a water-saturated medium: a detection strategy using ground penetrating radar*. Environ. Geosci., **7**, 169-176, doi: 10.1046/j.1529-0984.2000.74001.x.

Ludwig R., Gerhards H., Klenk P., Wollschläger U. and Buchner J.; 2009: *Electromagnetic methods in applied geophysics*. Institute of Environmental Physics, Heidelberg University, Heidelberg, Germany, 59 pp, <goo.gl/m94Pte>.

Marcak H. and Gołębiowski T.; 2008: *Changes of GPR spectra due to the presence of hydrocarbon contamination in the ground*. Acta Geophys., **56**, 485-504, doi:10.2478/s11600-008-0003-4.

Mukhlisin M. and Saputra A.; 2013: *Performance evaluation of volumetric water content and relative permittivity models*. The Scientific World J., ID421762, 7 pp., doi:10.1155/2013/421762.

Olofsson B., Jernberg H. and Rosenqvist A.; 2005: *Tracing leachates at waste sites using geophysical and geochemical modelling*. Environ. Geol., **49**, 720-732, doi:10.2478/s11600-008-0003-4.

Orlando L.; 2002: *Detection and analysis of LNAPL using the instantaneous amplitude and frequency of ground-penetrating radar data*. Geophys. Prospect., **50**, 27-41, doi:10.1046/j.1365-2478.2002.00288.x.

Pellerin L.; 2002: *Applications of electrical and electromagnetic methods for environmental and geotechnical investigations*. Surv. Geophys., **23**, 101-132, doi:10.1023/A:1015044200567.

Peplinski N.R., Ulaby F.T. and Dobson M.C.; 1995: *Dielectric properties of soils in the 0.3-1.3-GHz range*. IEEE Trans. Geosci. Remote Sens., **33**, 803-807, doi:10.1109/36.387598.

Porsani J., Filho W., Elis V., Shimeles F., Dourado J. and Moura H.; 2004: *The use of GPR and VES in delineating a contamination plume in a landfill site: a case study in SE Brazil*. J. Appl. Geophys., **55**, 199-209, doi:10.1016/j.jappgeo.2003.11.001.

Takahashi K., Igel J., Preetz H. and Kuroda S.; 2012: *Basics and application of ground-penetrating radar as a tool for monitoring irrigation process*. In: Kumar M. (ed), Problems, perspectives and challenges of agricultural water management, InTech. Open Sci., Rijeka, Croatia, pp. 155-180.

Topp G.C., Davis J.L. and Annan A.P.; 1980: *Electromagnetic determination of soil water content: measurements in coaxial transmission lines*. Water Resour. Res., **16**, 574-582, doi:10.1029/WR016i003p00574.

Corresponding author: Ahmed H. Mansi
Department of Civil and Environmental Engineering, Politecnico di Milano
Piazza Leonardo da Vinci 32, 20133 Milano, Italy
Phone: +39 02 2399 6505; fax: +39 02 2399 2206; email: ahmed.hamdi@polimi.it